Measuring ballast acceleration at track level

David Milne, Louis Le Pen, Geoff Watson, David Milne, William Powrie, Mick Hayward, Simon Morley

[1]Faculty of Engineering and the Environment
University of Southampton, United Kingdom
[2]Network Rail (High Speed) Ltd., London, United Kingdom

Abstract

The maximum operational speed of high-speed railways has increased considerably since the 1960s and is forecast to continue to rise. For example, routes being planned today expected to attain opening speeds of at least 360 km/h. When ballasted tracks are used for higher speeds, ballast flight may be of concern. The mechanisms of ballast flight are still not fully understood but it is hypothesized that ballast particles could become airborne owing to a combination of track bed excitation and air flow beneath a passing train. To understand better the mechanics of ballast flight measurements of individual particle accelerations are highly desirable, yet these are difficult to achieve. Trackside monitoring technologies generally provide data on the performance of the track superstructure and the track bed, not individual ballast particles. A novel measurement technique is presented. This is based on the use of low cost MEMs accelerometers embedded within individual ballast particles, which permits measurements of the acceleration of ballast particles in three axes. The utility of the method is demonstrated with reference to measurements from a section of well performing high speed track. Measurements of sleeper movements are also presented to demonstrate that there are differences in the motion of the ballast and the track superstructure.

Keywords: Ballast Acceleration, MEMS, Ballast Flight, Track Bed Vibration

1 Introduction

Many railways use crushed aggregate, known as ballast, to transfer loading on the track superstructure from passing traffic to the subgrade/formation below. Where ballasted track is used for high speed routes there is concern that ballast flight could affect railway operations. It is hypothesized that the combined effects of mechanical vibration of the track bed and the airflow beneath a passing train could cause individual particles to become airborne [1].

Measurements of the accelerations acting on individual ballast particles are needed to help understand this phenomena. However these are difficult to achieve using current trackside monitoring methods, which generally involve mounting a transducer or target on the sleepers or rail or other parts of the track superstructure [2-6]. More complex installations are capable of providing information throughout the track-bed [7], but can be costly especially in terms of the track access required.

None of these current systems provide measurements for individual ballast particles. Recent technological advances have led to the widespread availability of low cost Micro Electro Mechanical Systems (MEMS) and the miniaturisation of

data acquisition systems. Thus, it has become possible to design measurement systems capable of being deployed within the ballast or on the ballast surface without the requirement for costly equipment and/or intrusive track bed access.

In this study, three axis MEMS accelerometers were embedded within individual ballast particles. These were then used to measure accelerations of particles at the surface of the ballast result from passing trains on an operational railway line. These were taken during a period of trackside monitoring involving other measurement techniques. The new method provides data that shows whether the upward accelerations acting on the instrumented ballast, approach or exceed gravitational acceleration, which could give rise to ballast flight [1].

In this paper the MEMS device, the ballast particles selected and the method of embedding within a ballast particle are described. The method of data processing used to align the measurements with a track co-ordinate system is given. Results from field measurements at the ballast surface on an operational high speed railway are presented. Results for an individual train, peak acceleration values from multiple train passages and a comparison with sleeper end measurements obtained using geophones are shown.

2 Materials and methods

2.1 Device Selection

Several low cost MEMs transducers are commercially available. They are commonly used in everyday devices such as mobile phones to provide motion/directional sensitivity. MEMs devices are inexpensive: they cost at least an order of magnitude less expensive than alternative motion transducers such as piezo electric accelerometers or geophones. Traditionally MEMs devices have not been considered for use in research due to concerns about their reliability. However, advances in technology mean that this concern may no longer be justified.

After initial trials, the AXIVITY AX3 (Figure 1) was selected for the field study. This device consists of an ANALOG DEVICES ADXL345 digital tri-axial MEMS accelerometer and a miniature data acquisition system. The unit is sealed in an IP68 rated, 23 x 32.5 x 7.6 mm enclosure, with a micro USB connection. Measurements are stored internally for later download to a computer. The device was chosen for its standalone operation, small size, waterproofness, and programmable operational parameters. The sample rate and measurement range are selectable between 12.5 - 3200 Hz and ± 2 / 4 / 8 / 16 g respectively. [8-9].

Figure 1: Axivity AX3 [8]

MEMS accelerometers operate down to 0 Hz and therefore 'see gravity' hence may be calibrated by aligning each axis with gravity to confirm each reads 9.81 m/s^2. This check was carried out for each device used prior to embedment in ballast particles.

2.2 Embedding a transducer

Four ballast particles were selected. These had to be large enough to accept a slot suitable for the device enclosure while maintaining the integrity of the ballast particle. The particles selected are at the upper 30% sieve size of the ballast gradation [10]. All particles passed through a 50 mm sieve.

To embed the sensors, a slot was drilled into each stone using a Diamond tipped coring bit. Coolant was required to prevent damage to the drill and ballast particle and to facilitate cutting. An AX3 device was sealed into each slot using epoxy resin. The particles were painted white for easy identification on the track (Figure 3).

Figure 3: (a) Four Ballast Particles (b) Axivity AX3 embedded in ballast particle.

Embedding the sensor causes a change $\boldsymbol{\Delta}$ in the mass of the particle from $\boldsymbol{m_1}$ to $\boldsymbol{m_2}$, as the device and resin are of lower density than the parent rock. The changes in mass are recorded in Table 1. The volume of each particle $\boldsymbol{V}$ is recorded for completeness. The reductions in mass were less than 9 % for all particles.

Table 1: Change in particle masses due to embedding a sensor.

Particle	**V(m^3)**	**m_1 (g)**	**m_2 (g)**	**Δ (g)**	**%**

1	$1.12 \cdot 10^{-4}$	298	281	17	-5.7
2	$1.26 \cdot 10^{-4}$	334	316	18	-5.4
3	$1.14 \cdot 10^{-4}$	301	278	23	-7.6
4	$0.57 \cdot 10^{-4}$	198	181	17	-8.6

2.3 Orientations

It is possible to transform three orthogonal axes of measurement into a vertical and two orthogonal horizontal axes from any initial orientation, as follows.

At rest, zero horizontal and 9.81 m/s^2 vertical acceleration are expected. A rotational matrix R describes the transform between the measurement axes, X, Y, and Z and the expected horizontal and vertical accelerations:

$$\begin{pmatrix} X \\ Y \\ Z \end{pmatrix} = R \begin{pmatrix} 0 \\ 0 \\ 9.81 \end{pmatrix} \tag{1}$$

The rotational transform may be defined using three rotations: roll ϕ, pitch θ and yaw ψ, about reference longitudinal, lateral and vertical axes, respectively. A reference direction is required to determine yaw and a magnetometer (compass) is required to provide this. If a magnetometer is unavailable the horizontal component from one of the current acceleration axes may be taken as the reference direction. The rotations are non-commutative, so a convention must adapted regarding the order in which they are applied. A common convention is to apply roll, pitch then yaw. This convention allows roll and pitch to be determined as follows for zero assumed yaw, [11].

$$\tan\phi = \left(\frac{Y}{Z}\right) \tag{2}$$

$$\tan\theta = \frac{-X}{\sqrt{Y^2 + Z^2}} \tag{3}$$

2.4 Data Collection

All four instrumented particles were placed at track level on the surface of the crib ballast between the rails on an operational railway (Figure 4). They were placed with the measurement axes aligned approximately longitudinally with the running rails, laterally with the sleepers and vertically into the ground. Figure 5a defines the coordinate convention used in this paper for these devices, relative to the direction of travel on the railway line.

Waterproof insulation tape was used to cover the USB ports. The devices were configured to record continuously, sampling at 800 Hz for 12 hours. The operational range was set to ±8 g. After the devices had been recovered, data were downloaded

for processing. Individual pass-by events were identified and extracted from the dataset.

Measurements of sleeper vertical velocity were made concurrently using geophones [1]. The geophones were placed on the sleeper ends ahead of the bay containing the instrumented ballast (Figure 5b). They provide data that allows comparison between the behaviour of the track bed and superstructure (sleepers).

Figure 4: Instrumented ballast particles deployed on a railway line.

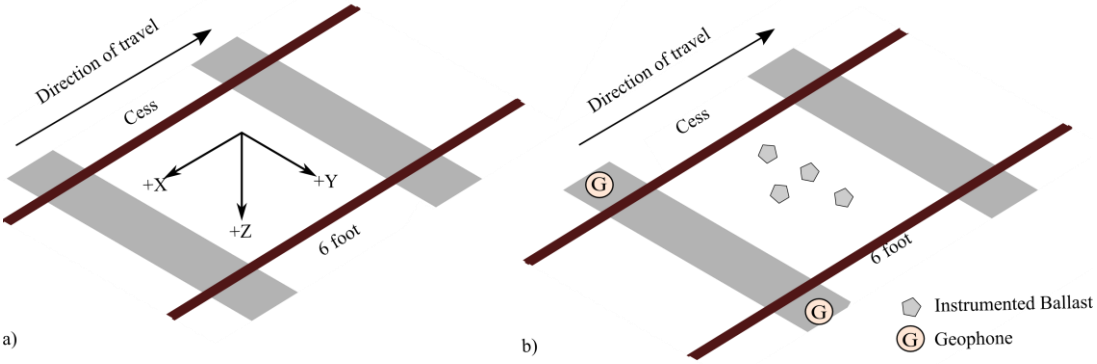

Figure 5: (a) sensor co-ordinate convention, (b) transducer positions

3 Results and discussion

Ballast accelerations were measured for passes of the same type of six vehicle train operating at speeds up to 225 km/h (62.5 m/s). In this section the results are evaluated in three ways:

- a typical result obtained with a train passing at 60 m/s is presented.
- the peak accelerations measured in the ballast are compared for multiple trains passages
- ballast and sleeper acceleration are compared for a single train passage.

3.1 Single Train

Figure 6 shows the calibrated measurements for each of the axes of ballast sensor 3. The mean accelerations show that this accelerometer was slightly inclined from its intended orientation so that the co-ordinate conventions for the measurement axes *X*, *Y* and *Z* of *longitudinal*, *lateral* and *vertical* are only approximately correct. However, the starting and final positions of the traces show that any rotation of the particle during this single train passage was minimal. Accelerations exceeding the at rest value are away from the direction of travel for the *X* axis, towards the 6 foot rail for the *Y* axis and into the ground for the *Z* axis (Figure 5a).

.

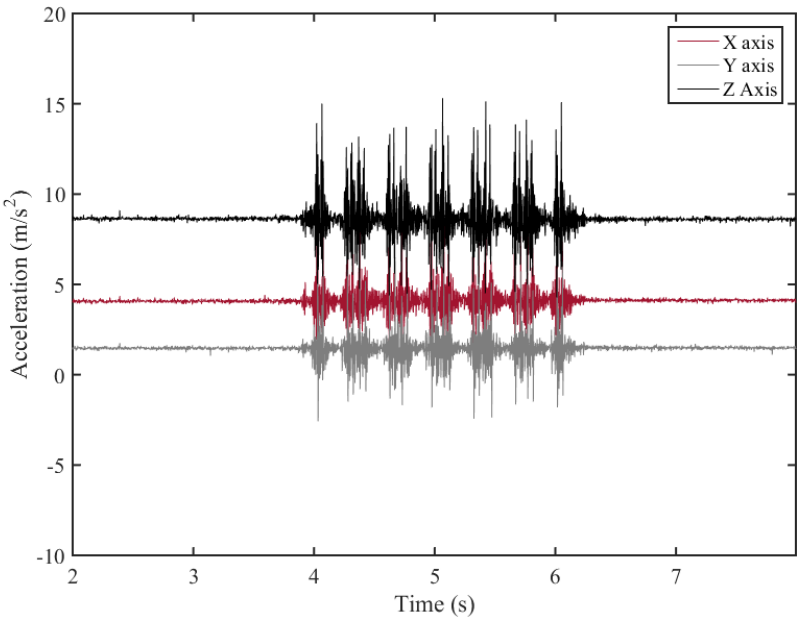

Figure 6: Accelerations from the three measurement axes of ballast sensor 3.

Figure 7 shows the accelerations after the orientation has been corrected. Accelerations exceeding 9.81 m/s^2 in the vertical direction are with gravity (i.e. downward).

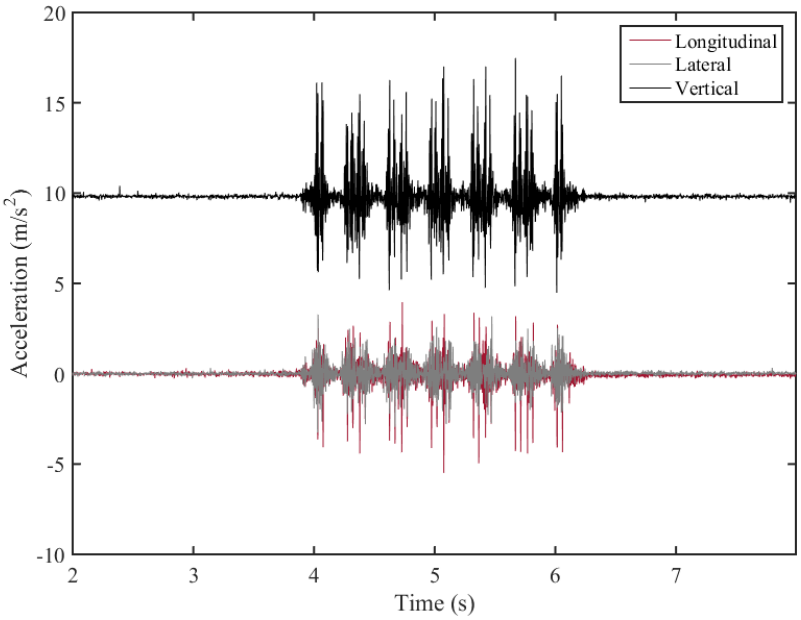

Figure 7: Results from ballast sensor 3 transformed into longitudinal, lateral and vertical components of acceleration.

The data from each of the measurement axes confirm that the transducer orientations were subsequently the same before and after each train passage (Figure 6). This indicates that the particle is unlikely to have moved and the axes transformation can reasonably be applied using the same offsets throughout the train passage.

Placement of the sensors with a measurement axis aligned with the direction of travel allowed acceleration components to be expressed using the track as a reference for the co-ordinate system. The results in Figure 7 show that vertical acceleration was greater than the horizontal accelerations. The dynamic components (net acceleration) of the downward acceleration was greater than for upward acceleration. For this train the net downward acceleration often exceeded 6 m/s^2 whereas the net upward acceleration was generally less than 5 m/s^2.

In the horizontal plane the longitudinal acceleration was greater than the lateral. The longitudinal acceleration was greatest in the direction of travel. As the instrumented particles were on the ballast surface the underbody airflow beneath the passing train may be responsible for these results [1]. The lateral acceleration had no dominant direction.

3.2 Peak accelerations for multiple trains

Results for the four similarly sized particles were found to have similar maximum upward net acceleration for the same train type for speeds between 57 and 62 m/s. Figure 7 shows the maximum and mean peak upward and downward accelerations found from 23 passages of a high speed commuter train. The mean peak accelerations are the averages of local maxima that exceeded a ±3 m/s^2 threshold.

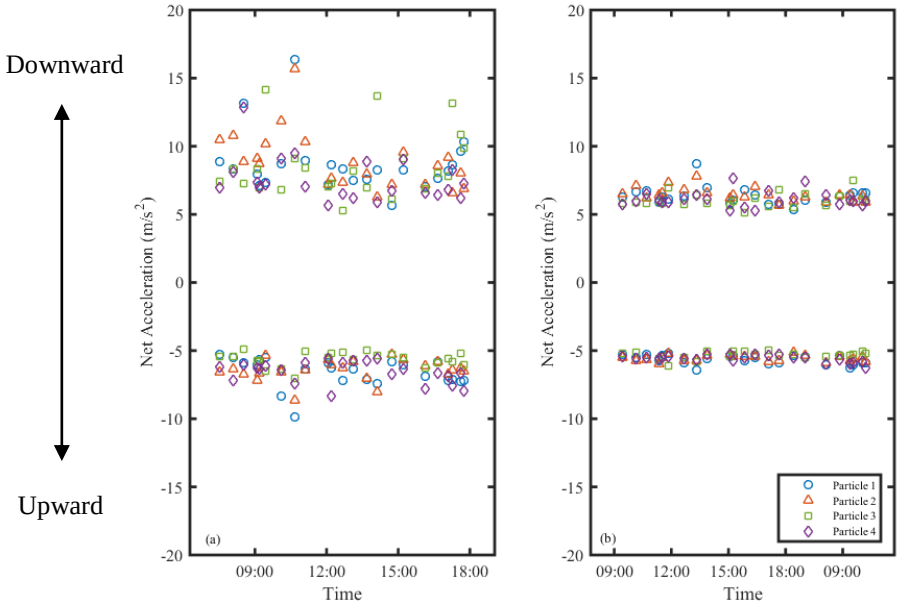

Figure 8: (a) Maximum peak net upward and downward acceleration in each train passage, (b) Mean peak net upward and downward acceleration for each train passage.

The mean peak upward acceleration was generally less than 6 m/s^2 for all the trains measured. There was more variation in maximum peak upward acceleration, which was generally than 7 m/s^2 (Figure 8). Larger accelerations were infrequent and were often isolated events within the train passage.

The magnitude of upward acceleration is of interest for studies of ballast flight phenomena. Upward accelerations that exceed gravitational acceleration are necessary for ballast flight [1]. No upward accelerations exceeding gravitational acceleration were measured. These results indicate that ballast particles of similar size to the embedded particles are unlikely to be susceptible to flight for the operating conditions at the test site, with this type of train.

3.3 Comparison with sleeper end measurements

Measurements of the velocity at the sleeper ends were differentiated to obtain accelerations, to enable comparison between the behaviour of the track bed and that of the track superstructure (Figure 9).

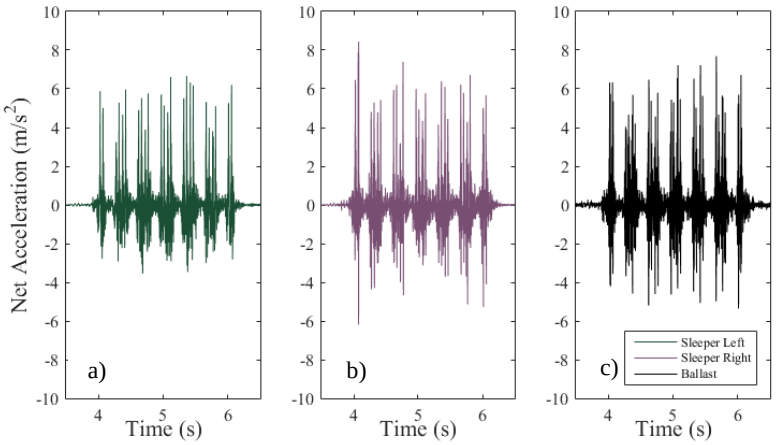

Figure 9: Vertical sleeper end (a & b) and ballast particle (c) acceleration time histories.

The Fourier transform for the vertical component of acceleration shows the frequency content of these measurements. The frequency spectra measured at sleeper ends are plotted next to the frequency spectra for the ballast accelleration measurements (Figure 10). Velocity data from the geophones were differentiated in the frequency domain for this comparison.

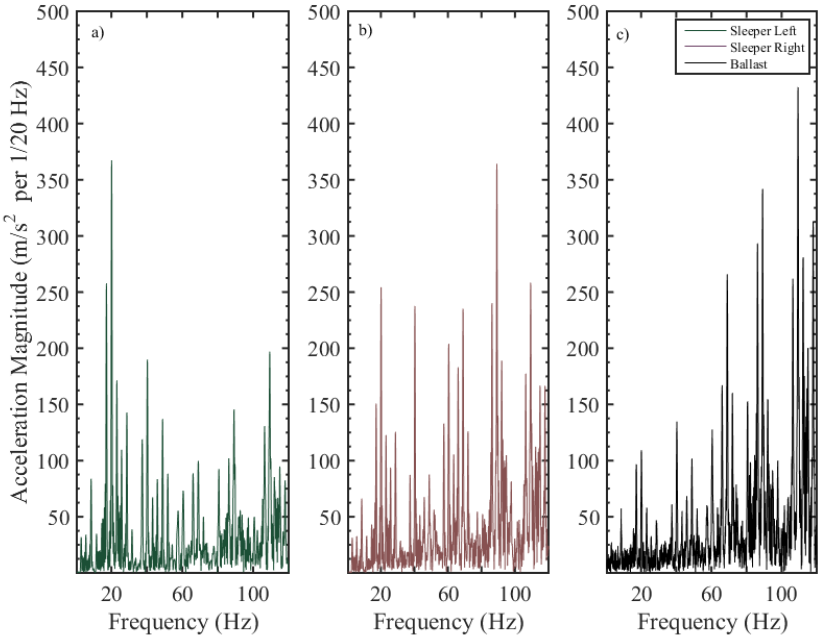

Figure 10: Fourier transform for (a & b) vertical sleeper end and (c) ballast particle accelerations

The acceleration time histories for the sleeper ends and ballast particle are broadly similar (Figure 9). The peak downward accelerations are close. The peak upward accelerations of the ballast are slightly greater than the sleepers. The spectral peaks for vertical acceleration measured at the ballast surface and the sleeper ends

occur at the same frequencies (Figure 10). For frequencies less than 60 Hz the magnitudes of the peaks for the sleeper measurements exceed those for the ballast. At frequencies above 60 Hz the magnitudes for the ballast exceed those for the sleeper measurements.

Measurements are likely to vary for different types of train and operating conditions as these will influence the combination of actions on the ballast particles. The shape and size of the ballast particles may also influence the actions on and response of each particle. The measurement approach developed may be used in future studies to build towards a more detailed understanding track bed ballast behaviour.

4 Conclusion

Improvements in MEMS technology and miniaturisation of data acquisition systems means it is now practicable to use embedded measurement systems to study the behaviour of railway ballast. Accelerometers and data acquisition systems were embedded in four ballast particles. The ballast particles were of similar size and shape and typical of the largest 30 % of a UK ballast gradation. The instrumented particles were placed on the surface of the ballast bed on an operational high speed railway. The measurements show the accelerations acting on the ballast particles under operational conditions.

Measured accelerations were consistent across all four particles for a number of passages of the same train type. Upward accelerations did not exceed gravitational, acceleration indicating ballast flight would be unlikely for normal operation for the particular trains evaluated at this site. The maximum amplitude of acceleration was similar for the ballast particles and at sleeper ends however differences in the behaviour of individual ballast particles and the sleeper ends were apparent in the spectra.

These results demonstrate the utility of this method for providing data to assist the study of in-situ ballast behaviour, including ballast flight phenomena and the differences between the behaviour of the track super structure and that of the ballast.

Acknowledgements

The research was funded by the Engineering and Physical Sciences Research Council (EPSRC) through the research grant Track Systems for High Speed Railways: Getting It Right (EP/K03765X) and the Industry Doctoral Training Centre in Transport and the Environment (EP/G036896/1).

References

[1] A.D. Quinn, M. Hayward, C.J. Baker, F. Schmid, J.A. Priest, W. Powrie, “A full-scale experimental and modelling study of ballast flight under high-speed trains”, Proceedings of the Institution of Mechanical Engineers, Part F: Journal of Rail and Rapid Transit, 224 (2010) 61-74.

[2] D. Bowness, A.C. Lock, W. Powrie, J.A. Priest, D.J. Richards, “Monitoring the dynamic displacements of railway track”, Proceedings of the Institution of Mechanical Engineers, Part F: Journal of Rail and Rapid Transit, 221 (2007) 13-22.
[3] J.A. Priest, W. Powrie, L.A. Yang, P.J. Grabe, C.R.I. Clayton, “Measurements of transient ground movements below a ballasted railway line”, Géotechnique, 60 (2010) 667-677.
[4] L. Le Pen, G. Watson, W. Powrie, G. Yeo, P. Weston, C. Roberts, “The behaviour of railway level crossings: Insights through field monitoring”, Transportation Geotechnics, (2014) 201-213.
[5] F. Lamas-Lopez, V. Alves-Fernades, Y.J. Cui, S. Costa D'Aguiar, N.C. Calon, J.C. Canou, A.M. Tang, A. Roubinet. Assessment of the double Integration method using accelerometers data for conventional railway platforms. In J. Pombo (Eds.), Proceedings of the second international conference on railway technology: Research, development and maintenance, Ajaccio, Civil-Comp Press, 2014.
[6] A. Paixão, C. Alves Ribeiro, N. Pinto, E. Fortunato, R. Calçada. On the use of under sleeper pads in transition zones at railway underpasses: experimental field testing. Structure and Infrastructure Engineering, (2014). 1-17.
[7] T.D. Stark, S.T. Wilk, Root cause of differential movement at bridge transition zones, Proceedings of the Institution of Mechanical Engineers, Part F: Journal of Rail and Rapid Transit, (2015).
[8] Analog Devices, “ADXL345 Datasheet”, 2009.
[9] Axivity, “AX3 User Guide”, Newcastle, 2012.
[10] Network Rail, “NR/L2/TRK/8100 Railway Ballast and stoneblower aggregate”, London, 2009.
[11] M. Pedley, “Tilt sesnsing using a three-axis accelerometer”, Freescale Semiconductor, 2007.